Cite this: *Phys. Chem. Chem. Phys.*, 2012, **14**, 2774–2783

www.rsc.org/pccp

**PAPER**



# Comparison of the photoelectrochemical oxidation of methanol on rutile $TiO_2$ (001) and (100) single crystal faces studied by intensity modulated photocurrent spectroscopy

**Amira Y. Ahmed,[ab] Torsten Oekermann,*[a] Patrick Lindner[c] and Detlef Bahnemann[c]**

***Received 29th October 2011, Accepted 4th January 2012***
**DOI: 10.1039/c2cp23416e**

The photooxidation of methanol as a model substance for pollutants on rutile $TiO_2$ (001) and (100) surfaces was investigated using intensity modulated photocurrent spectroscopy (IMPS). The results are analyzed in view of the influence of the surface structure, the methanol concentration and the electrode potential on the rate constants of charge transfer and recombination. The obtained results have been explained with a model combining the theory of IMPS for a bulk semiconductor surface and the nature of the surface-bound intermediates (alternatively mobile or immobile $OH^{\bullet}$ radicals). The results indicate that water photooxidation proceeds *via* mobile $OH^{\bullet}$ radicals on both surfaces, while methanol addition gives rise to the involvement of immobile $OH^{\bullet}$ radicals on the (100) surface. Detailed analysis in view of the surface structures suggests that the latter observation is due to efficient electron transfer from bridging $OH^{\bullet}$ radicals on the (100) surface to methanol, while coupling of two of these radicals occurs in the absence of methanol, making them appear as mobile $OH^{\bullet}$ radicals. In the case of the (001) surface, the coupling reaction dominates even in the presence of methanol due to the smaller distance between the bridging $OH^{\bullet}$ radicals, leading to more efficient water oxidation, but less efficient methanol photooxidation on this surface.

## Introduction

Considerable attention has been paid to photocatalytic reactions occurring on $TiO_2$ surfaces under UV-light illumination especially in view of the purification of water by the decomposition of hazardous chemicals.[1–3] It is generally accepted that photooxidation in aqueous electrolytes proceeds *via* surface $OH^{\bullet}$ radicals formed by transfer of photogenerated holes in the valence band of $TiO_2$ to surface $OH^-$ or water species. The strong oxidizing power of the photogenerated holes, the chemical inertness of the material and its non-toxicity have made $TiO_2$ a superior photocatalyst. However, despite the tremendous amount of attention paid to photocatalytic processes involving $TiO_2$ from both applied and fundamental viewpoints, many details of the reaction mechanisms are still not fully understood.[4] For example, to further improve the performance of $TiO_2$-based photocatalysts, a thorough knowledge of the photocatalytic properties of different crystal modifications and surfaces is of high importance.

In principle, photocatalytic reactions at a semiconductor surface can be regarded as irreversible photoelectrochemical reactions. In fact, the use of photoelectrochemical cells has been proposed as an alternative for the decomposition of pollutants in recent years.[5–7] Compared to reactors containing only the photocatalyst and the solution to be cleaned, one advantage of such a setup is that the photogenerated electrons can be removed from the photocatalyst surface through an external electrical circuit, so that no electron acceptor is necessary to remove them. Furthermore, the hole concentration at the surface of the photocatalyst can be tuned by applying different potentials to the electrode *vs.* a reference electrode with stable potential. Details of many photoelectrochemical reactions in general have been successfully investigated using dynamic photoelectrochemical methods.[8] Photocurrent transient methods[9–15] and intensity modulated photocurrent spectroscopy (IMPS),[8,10,16–22] where the working electrode is illuminated with sinusoidally modulated light, have been used for this purpose in particular. These methods can be employed to measure the rate constants of charge transfer and recombination processes occurring at the semiconductor/electrolyte interfaces.[23–26] However, a detailed study comparing different $TiO_2$ single crystal surfaces by using these methods has not been conducted so far.

[a] *Institute of Physical Chemistry and Electrochemistry, Leibniz Universität Hannover, Callinstrasse 3A, 30167 Hannover, Germany. E-mail: torsten.oekermann@pci.uni-hannover.de*
[b] *Department of Chemistry, Faculty of Science, Sohag University, Sohag 82524, Egypt*
[c] *Institute of Technical Chemistry, Leibniz Universität Hannover, Callinstrasse 5, 30167 Hannover, Germany*

Herein we report the results of IMPS measurements which have been performed comparatively at rutile $TiO_2$ (001) and (100) surfaces, in order to study their photoelectrochemical kinetics towards methanol photooxidation in a semi-quantitative way. Methanol was chosen as a typical model substance for organic pollutants.[27–29] The IMPS measurements have been performed in aqueous electrolytes under variation of the methanol content and the electrode potential, which are expected to be the factors most strongly influencing charge transfer and recombination at the surface. The results reveal quite significant differences between the two surfaces concerning the dominating mechanism of photooxidation, leading to significantly different rate constants for water and methanol photooxidation. The differences are explained by the structural differences of the two surfaces on an atomic level.

## Experimental section

### Preparation of rutile $TiO_2$ (001) and (100) electrodes

Single crystal rutile $TiO_2$ wafers with a size of 10 × 10 × 0.5 $mm^3$ exhibiting polished (100) or (001) surfaces, respectively, on one side were purchased from K&R creation Co., Japan and cut into pieces of 5 × 5 × 0.5 $mm^3$. To achieve n-type doping by oxygen vacancies, the wafers were exposed to a stream of hydrogen gas at 600 °C for 2 h. Electrodes were fabricated by connecting copper wires to the surfaces opposite to the polished surfaces of these wafers using conductive epoxy resin. The copper wires were covered with glass tubes, and the connections between the glass tubes and the wafers except the polished surfaces were sealed with non-conductive epoxy resin (Araldite Rapid, Ciba Geigy).

Prior to the electrochemical measurements a part the electrode surfaces has been photoetched to remove the thin inactive surface layer formed during the $H_2$ treatment. Photoetching was carried out in 0.05 M $H_2SO_4$ using a three-electrode photoelectrochemical cell with a Pt counter electrode and an Ag/AgCl/NaCl(sat) reference electrode as previously reported by Imanishi *et al.*[30,31] The electrode potential was kept at +2.5 V during UV illumination with a 250 W Xe lamp for approximately 15 s, the incident light intensity at the electrode surface being 5 mW $cm^{-2}$.

### Electrochemical measurements

All electrochemical measurements were carried out at room temperature in a 30 mL glass cell with a quartz window, using a rutile $TiO_2$ (001) or (100) substrate as a working electrode, an Ag/AgCl/NaCl (sat) reference electrode, a Pt counter electrode and 20 mL electrolyte solution. Data acquisition was performed with a Zahner IM6e electrochemical workstation. A 250 W Xe lamp served as a light source during cyclic voltammetry, the incident light intensity at the electrode surface being 5 mW $cm^{-2}$. A UV-light emitting diode (UV-LED, 375–380 nm) driven by a Zahner PP210 potentiostat connected to the electrochemical workstation was used as a light source for IMPS exhibiting a dc light intensity of 0.38 mW $cm^{-2}$ at the electrode surfaces. The light intensity of the UV-LED was modulated sinusoidally by ±8%, as measured with a calibrated Eppley thermopile. All solutions were prepared using reagent grade chemicals unless mentioned otherwise. The supporting electrolyte was 0.1 M KCl dissolved in ultra-pure water. Aqueous methanol solutions were prepared by addition of pure methanol (Roth, analytical grade 99.9%).

## Theory

### General IMPS response

In intensity modulated photocurrent spectroscopy (IMPS), the working electrode is illuminated by a modulated light source. The amplitude of the illumination function is chosen not to exceed *ca.* ±10% to ensure that the system remains near a steady state during the measurement. The phase shift $\varphi$ of the resulting photocurrent with respect to the light modulation and its amplitude $A$ are measured for different modulation frequencies $f$. Similar to impedance measurements, the results are usually shown in Bode plots ($\varphi$ and $A$ *vs.* $f$) or, more commonly, in complex plane plots, where a semicircle appears in the positive/positive quadrant as schematically shown in Fig. 1(b).[8,10]

The modulated illumination leads to a modulated flow of photogenerated minority carriers (holes in this case), the so-called Gärtner flux $g_1$, towards the surface, where they can undergo charge transfer to the electrolyte (rate constant $k_{tr}$) or recombination with electrons (rate constant $k_{rec}$) as illustrated in Fig. 1(a). The relaxation in the concentration of photogenerated holes at the semiconductor surface is characterized by $f_{max}$, which is the frequency at the maximum of the semicircle. The rate constants $k_{tr}$ and $k_{rec}$ can be calculated according to[26]

$$2\pi f_{max} = k_{tr} + k_{rec} \quad (1)$$

$$\frac{I_1}{I_2} = \frac{k_{tr}}{k_{tr} + k_{rec}} \quad (2)$$

where $I_1$ and $I_2$ are the low and high frequency intersections of the semicircle with the real axis (Fig. 1(b)). The low frequency limit $I_1$ represents the differential steady-state photocurrent increase due to a differential increase in the light intensity,[8] while the high frequency intercept $I_2$ represents the amplitude of the Gärtner flux.[32]

The simple data analysis based on the values of $f_{max}$, $I_1$ and $I_2$ neglects the influence of $RC$ attenuation, which is usually recognized as a continuation of the IMPS complex plane plot in the positive/negative quadrant towards very high frequencies, but can also lead to a distortion of the IMPS response in the

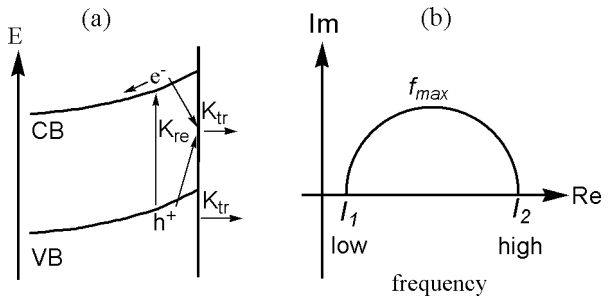


**Fig. 1** (a) Illustration of processes involving photogenerated holes at the electrode surface. (b) Scheme of an IMPS complex plane plot.

positive/positive quadrant if the difference between its time constant ($\tau = 1/(2\pi f_{max})$) and $RC$ is relatively small. This may lead to significant errors in the determination of $I_2$, $k_{tr}$ and $k_{rec}$. A much more accurate determination of $k_{tr}$ and $k_{rec}$ is possible by fitting the experimental data to a transfer function describing the frequency dependent IMPS response including the effect of $RC$ attenuation for a given case. It has been shown that the IMPS response in the given case is expressed by

$$\frac{j(\omega)}{g_1} = \frac{k_{tr} + i\omega\frac{C}{C_{sc}}}{k_{tr} + k_{rec} + i\omega}\left(\frac{1}{1 + i\omega RC}\right) \quad (3a)$$

with

$$C = \frac{C_{SC}C_H}{C_{SC} + C_H} \quad (3b)$$

where $R$ is the series resistance, $C_{SC}$ and $C_H$ are the space charge and the Helmholtz capacitances, respectively, $i$ is the imaginary unit and $\omega = 2\pi f$.[33] The second term (in brackets) in eqn (3a) describes the $RC$ attenuation, while the first term describes the response due to the processes illustrated in Fig. 1(a).

Note that the rate parameters $k_{tr}$ and $k_{rec}$ are identical with the true charge transfer and recombination rate constants only in the simplest case of one-electron charge transfer processes (Fig. 1(a)). In the case of multi-electron transfer-reactions, $k_{tr}$ and $k_{rec}$ have to be interpreted as phenomenological rate parameters, which are functions of the rate constants associated with the elementary steps, while, however, not being identical with them. This is also the case for the photooxidation of water and methanol studied in this paper. An extended IMPS model for the present study is therefore introduced in the following section.

### Photooxidation mechanism

Since the photoelectrochemical measurements have been carried out employing aqueous solutions, there is, in principle, a competition between the photooxidation of methanol and water at the $TiO_2$ surface. The details of the photooxidation processes are still not fully understood. For example, there is still a debate whether the photooxidations proceed *via* mobile or immobile $OH^\bullet$ radicals. Since both types of species are potentially active towards oxidation of organic compounds, they will be hereafter called surface hydroxyl radicals ($OH^\bullet_s$) unless the difference in surface structure of the two faces will be discussed. Regardless of the nature of the photogenerated radical species, methanol has often been employed as a scavenger for photogenerated radicals in order to determine the quantum yield or the photonic efficiency of radical generation at the $TiO_2$ surface.[34–36]

Peter *et al.*[37] have developed a phenomenological IMPS analysis to describe multistep electron transfer reactions that also considers the involvement of mobile and immobile intermediates. The general mechanisms considered are of two types (Case I and Case II) consisting of the following elementary steps:

$$A + h^+ \xrightarrow{k_1} X^+ \quad (4a)$$

followed by

$$X^+ + h^+ \xrightarrow{k_2} B^{2+} \ \text{(Case I)} \quad (4b)$$

or by

$$X^+ + X^+ \xrightarrow{k_4} A + B^{2+} \ \text{(Case II)} \quad (4c)$$

Recombination in both cases occurs by the reaction

$$X^+ + e^- \xrightarrow{k_3} A \quad (4d)$$

Here $k_1$ and $k_3$ are pseudo-first order rate constants, A is a hole trapping site in the semiconductor crystal lattice, $B^{2+}$ is the final product and $X^+$ is an intermediate, which is mobile and can therefore react with another $X^+$ (eqn (4c), Case II) or immobile and therefore reacts by catching a hole (eqn (4b), Case I). In the system under investigation, the hole trapping sites A can be described as $OH^-$ anions or water molecules at the $TiO_2$ surface and $X^+$ as the surface hydroxyl radicals $OH^\bullet_s$, which are further oxidized to oxygen:

$$OH^-/(H_2O - H^+) + h^+ \xrightarrow{k_1} OH^\bullet_s \quad (5a)$$

$$OH^\bullet_s + h^+ \xrightarrow{k_2} \tfrac{1}{2}O_2 + H^+ \ \text{(Case I)} \quad (5b)$$

$$OH^\bullet_s + H^+ + e^- \xrightarrow{k_3} H_2O \quad (5c)$$

$$OH^\bullet_s + OH^\bullet_s \xrightarrow{k_4} OH^- + \tfrac{1}{2}O_2 + H^+ \ \text{(Case II)} \quad (5d)$$

Due to the presence of methanol in the electrolyte, another reaction with a fifth rate constant rate needs to be added to this system, taking into account the reaction between methanol and $OH^\bullet_s$:

$$OH^\bullet_s + CH_3OH \xrightarrow{k_5} {}^\bullet CH_2OH + H_2O \quad (5e)$$

This reaction opens a new charge-transfer route for the intermediate, so that charge-transfer from the intermediate would proceed with a rate constant of $k_2 + k_5$ (instead of $k_2$) in Case I and with a rate constant of $k_4 + k_5$ (instead of $k_4$) in Case II. Based on the model of Peter *et al.*[37] the following expressions for $k_{tr}$ and $k_{rec}$ as functions of $k_1$ to $k_5$ are obtained:

$$\textit{Case I}: \ k^I_{tr} = \frac{2(k_2 + k_5)(k_1p_0 + k_3X_0)}{k_1 + (k_2 + k_5)(p_0 + X_0) + k_3} \quad (6a)$$

$$k^I_{rec} = \frac{k_3(k_1 - (k_2 + k_5)X_0)}{k_1 + (k_2 + k_5)(p_0 + X_0) + k_3} \quad (6b)$$

$$p_0 = \frac{g}{k_1 + k_2X_0} \quad (6c)$$

$$X_0 = \frac{k_1p_0}{k_2p_0 + k_3} \quad (6d)$$

$$\textit{Case II}: \ k^{II}_{tr} = \frac{8k_1(k_4 + k_5)X_0}{k_1 + 8(k_4 + k_5)X_0 + k_3} \quad (6e)$$

$$k^{II}_{rec} = \frac{k_1k_3}{k_1 + 8(k_4 + k_5)X_0 + k_3} \quad (6f)$$

$$X_0 = \frac{-k_3 + \sqrt{k_3^2 + 16k_4g_0}}{8k_4} \quad (6g)$$

 

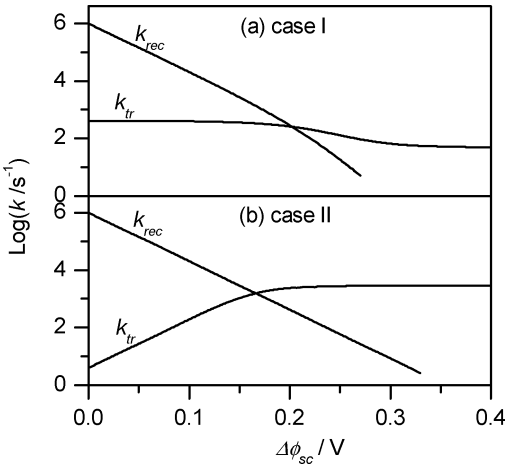


**Fig. 2** Phenomenological rate constants as a function of the band bending for (a) Case I and for (b) Case II. $k_1 = 10^{-10}$ s$^{-1}$, $k_2 = 10^{-3}$ cm$^2$ s$^{-1}$, $k_3^0 = 10^5$ s$^{-1}$, $k_4 = 10^{10}$ s$^{-1}$, $g = 10^{14}$ cm$^{-2}$ s$^{-1}$, $\beta = 1$. These simulations have been adapted from ref. 37.

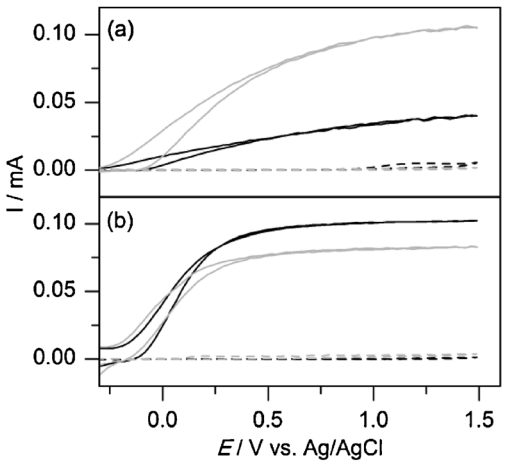


**Fig. 3** *I–V* curves measured at (a) (001) and (b) (100) surfaces of rutile $TiO_2$ in the dark (dashed lines) and under illumination (solid lines) with a 250 W Xe lamp in 0.1 M KCl (aq), scan rate = 200 mV s$^{-1}$. The measurements have been carried out before (black) and after (grey) photoetching.

Here $X_0$ and $p_0$ are the surface concentrations of the surface intermediate and holes, respectively. The rate constant for recombination, $k_3$, depends on the electron concentration at the surface of the $TiO_2$ electrode, which itself depends on the electrode potential according to the equation

$$k_3 = k_3^0 \exp\left(\frac{-\beta q \Delta\phi_{SC}}{k_B T}\right) \quad (7)$$

where $k_B$ is the Boltzmann constant, $\beta$ is an empirical factor associated with Fermi-level pinning, $q$ is the elementary charge and $k_3^0$ is the value of $k_3$ at the flatband potential $E_{FB}$, *i.e.*, when the potential drop in the space charge layer $\Delta\phi_{SC} = E - E_{FB} = 0$.[37] As seen in the results of model calculations shown in Fig. 2, the potential dependence of $k_{tr}$ is a good indicator to distinguish between Case I and Case II, since it shows a falling trend towards higher band bending in Case I, while it increases to a saturation value in Case II. Concerning $k_{rec}$, a falling trend is seen in both cases (with a slope of (59 mV)$^{-1}$ on a log$k$ *vs.* potential plot in Case II, but with a steeper slope in Case I).

## Results and discussion

### *I–V* curves

*I–V* curves of (001) and (100) $TiO_2$ electrodes have been measured to determine the potentials of photocurrent onset and photocurrent saturation. In general, IMPS measurements are usually performed in the photocurrent onset region, since recombination and therefore the typical semicircle in the IMPS complex plane plot disappears in the saturation region. Furthermore, the measurements have been performed using electrodes before and after photoetching in order to identify the best pre-treatment methods for the respective surfaces.

Fig. 3 shows the *I–V* curves of (001) (a) and (100) (b) surfaces in the dark and under illumination before and after photoetching, respectively, measured in aqueous KCl. As it is typical for n-type semiconductors, all electrodes show anodic photocurrents towards positive potentials corresponding to the photooxidation of water. A rather fast increase of the photocurrent to a saturation level is observed towards positive potentials for the (100) electrodes. The increase is considerably slower in the case of the (001) electrode, where a saturation level is still not reached at the highest potential of 1.5 V. This is mainly due to the formation of an inactive thin surface layer during $H_2$ treatment as previously reported[30] and supported here by scanning electron microscopy measurements (see Fig. 4a and b). For this reason, it was essential to remove this inactive film by photoetching before the IMPS measurements. We were not able to obtain a well-resolved IMPS response from the (001) surface without photoetching. After photoetching of the (001) electrode, a three-fold increase of the current under illumination is observed. At the same time, the current decreases in the dark. Both observations may be explained by the presence of surface states initially present at the electrode surface, which may promote charge transfer in the dark while, however, leading to an increased recombination of photogenerated

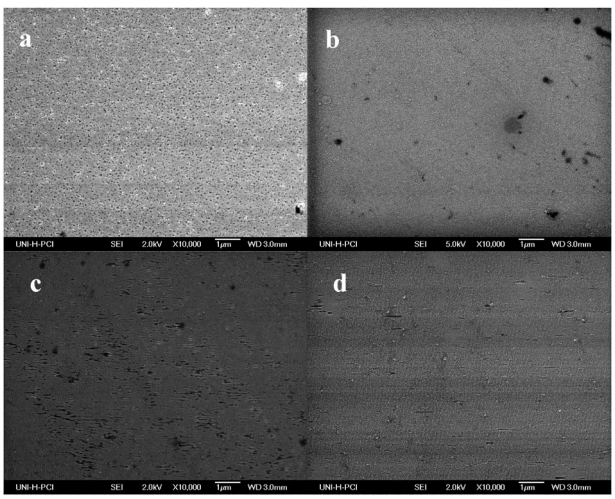


**Fig. 4** SEM images of $TiO_2$ (a) (001) before photoetching, (b) (001) after photoetching, (c) (100) before photoetching, and (d) (100) after photoetching.

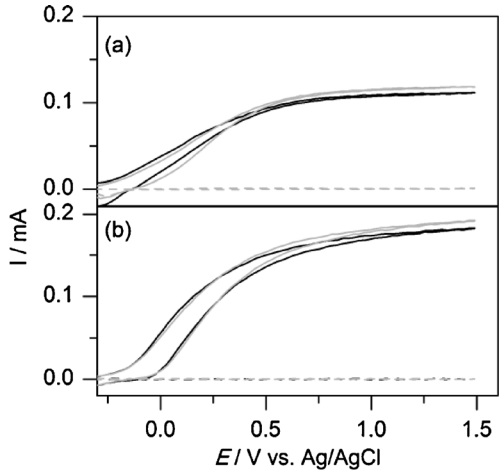


**Fig. 5** *I–V* curves measured at rutile $TiO_2$ (a) (001) and (b) (100) surfaces in the dark (dashed lines) and under illumination (solid lines) with a 250 W Xe lamp in 0.1 M KCl (aq), scan rate = 200 mV $s^{-1}$. The measurements have been made before (black) and after (grey) addition of 1 vol% methanol.

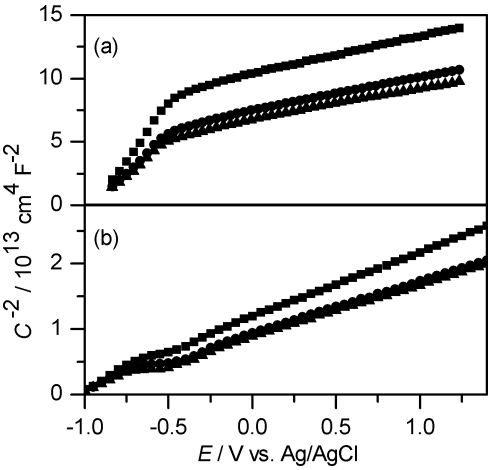


**Fig. 6** Influence of methanol addition on the Mott–Schottky plots of rutile $TiO_2$ (a) (001) and (b) (100) electrodes: 0% (■), 1% (●) and 10% (▲) methanol.

holes under illumination. On the other hand, almost the opposite behaviour is seen for the (100) electrode. Here the current under illumination slightly decreases after photoetching, while the current in the dark shows an increase. Concerning the appearance of the films in the SEM, no significant change is apparent due to the photoetching in the case of (100) (Fig. 4c and d). Following these results, photoetched (001) electrodes and non-photoetched (100) electrodes have been employed for all further investigations.

No changes induced by photoetching are observed in Fig. 3 concerning the photocurrent onset regions and the shapes of the curves in this region. All electrodes exhibit a photocurrent onset at about −0.3 V *vs.* Ag/AgCl, with an exponential increase up to about 0 V *vs.* Ag/AgCl. In this region, the flatband potential of $TiO_2$ is expected, since its conduction band edge was reported to be at −4.3 eV *vs.* vacuum level, which corresponds to a potential of *ca.* −0.4 V *vs.* Ag/AgCl. Towards more positive potentials the photocurrent *vs.* potential curves exhibit saturation behaviour.

Fig. 5 illustrates the influence of methanol addition on the *I–V* curves as observed at both (001) and (100) electrodes. The most important feature observed in this figure is that the increase of the photocurrent induced by the methanol addition is rather small (less than 10%) at both surfaces, indicating a low ratio of photocurrent doubling under the given conditions. It is important to note that the *I–V* curves in Fig. 5 have been measured employing a high light intensity Xe lamp whereas the IMPS measurements have been measured employing a LED with rather low light intensity. With decreasing light intensity the ratio of the current doubling is even expected to be further decreased as previously reported by Fermin *et al.*[38]

### Mott–Schottky plots

Mott–Schottky plots measured at rutile (001) and (100) surfaces at different methanol contents in the electrolyte are shown in Fig. 6. The corresponding doping densities $N_D$ and flatband potentials $E_{FB}$ have been calculated from the slopes and intersections with the potential axis according to the Mott–Schottky relationship

$$I/C^2 = \frac{2}{\varepsilon_0 \varepsilon q N_D A^2}(E - E_{FB} - kT/q) \qquad (8)$$

where $C$ is the capacitance, $\varepsilon$ is the dielectric constant of the semiconductor, $\varepsilon_0$ the vacuum permittivity and $N_D$ the doping density. The $N_D$ values, which have been calculated assuming a dielectric constant of rutile $TiO_2$ of 173,[39] are summarized in Table 1. For the determination of $E_{FB}$ in cases of highly doped semiconductor electrodes ($N_D \geq 10^{19}$ $cm^{-3}$) it has to be considered in the analysis of Mott–Schottky plots that the space charge capacitance can reach values comparable to that of the Helmholtz layer capacitance. This leads to an additional shift of the intersection with the potential axis by $\varepsilon\varepsilon_0 q N_D/(2C_H^2)$ with respect to the flatband potential, while the slope is not affected.[40] For our electrodes we calculated correction terms of 0.018 V and 0.012 V for (001) and (100) faces, respectively, based on respective $C_H$ values of 20 μF $cm^2$ and 3 μF $cm^2$ as obtained by fitting the IMPS results (see the next section).

Table 1 summarizes the values of $E_{FB}$ and $N_D$ for rutile (001) and (100) faces in the absence and presence of methanol. Comparison of the $E_{FB}$ values reveals that the addition of methanol to the electrolyte does not lead to a significant shift in the case of both surfaces. Since adsorption of ions or polar molecules usually leads to a shift of $E_{FB}$, this result strongly suggests that methanol adsorption on the electrodes does not occur in this case, *i.e.*, that the adsorption of water molecules

**Table 1** Flatband potentials $E_{FB}$ and doping densities $N_D$ extracted from Mott–Schottky plots measured at a frequency of 5 kHz in 0.1 M KCl (aq)

| $TiO_2$ surface | Methanol content | $E_{FB}$/V *vs.* Ag/AgCl | $N_D/10^{19}$ $cm^{-3}$ |
|---|---|---|---|
| (001) | 0 | −1 | 0.526 |
| (001) | 1 vol% | −1 | 0.585 |
| (001) | 10 vol% | −1 | 0.628 |
| (100) | 0 | −0.95 | 1.31 |
| (100) | 1 vol% | −0.94 | 1.61 |
| (100) | 10 vol% | −0.94 | 1.62 |

 

or $OH^-$ ions is much stronger than that of methanol. Hence, direct charge transfer of free photogenerated holes from the valence band of $TiO_2$ to methanol is unlikely to happen, *i.e.*, oxidation of methanol can only occur *via* $OH^{\bullet}_s$ radicals as described in the Theory section (*vide supra*).

The $N_D$ values for both faces are of the order of magnitude expected from the fact that the doping density should be a bulk property and doping in a $H_2$ atmosphere has been carried out in the same way for all samples. The observed differences in the $N_D$ values are therefore probably caused by dissimilarities in the surface roughness, leading to diverse microscopic surface areas.

The doping densities can be used to calculate the width of the space charge layer $W$ at the surface of the $TiO_2$ electrodes employing the following equation

$$W = \sqrt{\frac{2\Delta\phi_{SC}\varepsilon\varepsilon_0}{qN_D}} \qquad (9)$$

Based on the values of $E_{FB}$ and $N_D$ given in Table 1, the thickness of the space charge layer is calculated to be between 50 and 60 nm for the (001) face and between 27 and 33 nm for the (100) face at potentials between −0.3 and 0 V *vs.* Ag/AgCl, respectively. Since the light absorption coefficient of rutile is around $4 \times 10^4$ $cm^{-1}$ in the wavelength region used for illumination of the employed electrodes during the IMPS measurements,[40] it follows that only between 11% (at −0.3 V *vs.* Ag/AgCl) and 13% (at 0 V *vs.* Ag/AgCl) of the incident light is absorbed in the space charge region of the (001) face, whereas 6% (at −0.3 V *vs.* Ag/AgCl) to 7% (at 0 V *vs.* Ag/AgCl) are absorbed in the space charge layer of the (100) face. As will be seen in the IMPS results (*vide infra*), this limits the external quantum efficiency of the photoelectrochemical reactions investigated in this study, since only holes that are photogenerated within the space charge region or in its utmost vicinity reachable by diffusion will be transferred to the electrode surface and thus contribute to the Gärtner flux.

### Typical IMPS plots

Some typical IMPS responses in the positive/positive part of the complex plane measured in this study are shown in Fig. 7 and 8. Fig. 7 illustrates the influence of the electrode potential in the case of rutile (001). Towards positive potentials, a significant

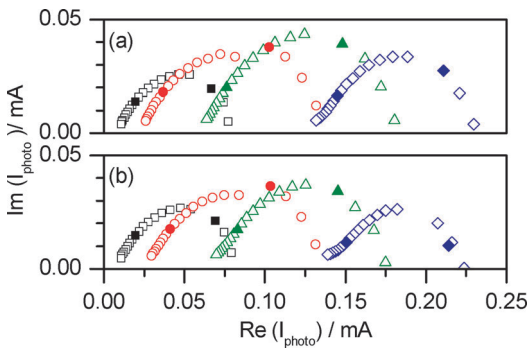


**Fig. 7** IMPS measured at the rutile $TiO_2$ (001) surface in aqueous 0.1 M KCl (a) before and (b) after addition of 1 vol% methanol at potentials of −0.3 V *vs.* Ag/AgCl (□), −0.2 V *vs.* Ag/AgCl (○), −0.1 V *vs.* Ag/AgCl (△) and 0 V *vs.* Ag/AgCl (◇), solid symbols indicate measurements at 63 and 6.3 Hz, respectively.

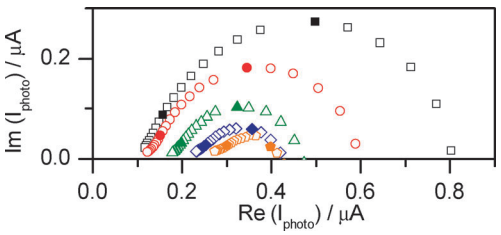


**Fig. 8** IMPS measured at the rutile $TiO_2$ (100) surface in aqueous 0.1 M KCl with methanol concentrations of 0 (□), 1 vol% (○), 5 vol% (△), 10 vol% (◇) and 15 vol% (⬠) at −0.2 V *vs.* Ag/AgCl, solid symbols indicate measurements at 63 and 6.3 Hz, respectively.

increase of $I_1$ is observed, while $I_2$ also increases, however, to a lesser extent. According to eqn (2), this observation translates into a decrease in $k_{rec}$ relative to $k_{tr}$. Comparison of parts (a) and (b) in Fig. 7 reveals that the addition of methanol (Fig. 7b) intensifies this trend as is evident from the tendency towards smaller semicircles. Obviously, the presence of methanol as an additional reactant leads to an increase in $k_{tr}$. A clearer illustration of the impact of the methanol concentration can be found in Fig. 8, where IMPS plots measured with different methanol concentrations at a (100) electrode can be seen.

Another interesting observation for both series of experiments is the increase of $I_2$ towards more positive potentials. This indicates an increase in the Gärtner flux and thereby the external quantum efficiency, which can be attributed to the increasing width of the space charge layer as discussed in the foregoing section. A differential quantum efficiency of 1 under the given conditions (modulation of the light intensity with an amplitude of 0.03 mW $cm^{-2}$) would translate into a photocurrent amplitude of 1.82 μA $cm^{-2}$, assuming that 20% of the incident light is lost by reflection,[39] so that the $I_2$ values seen in Fig. 7 correspond to quantum efficiencies between 4% and 13%. The latter value matches well with the value calculated based on light absorption within the space charge layer at 0 V *vs.* Ag/AgCl, whereas the former is lower than the calculated value, indicating that the rate of recombination within the space charge layer is higher at a potential of −0.3 V *vs.* Ag/AgCl. This is actually expected due to the increasing electron concentration at the electrode surface towards more negative potentials.

A more detailed analysis of the IMPS results has been performed by fitting all IMPS plots to eqn (3). Fig. 9 shows an example of a full experimental IMPS response (including the part in the positive/negative quadrant measured at high frequencies) and the corresponding fit according to the model. The fitted values were $k_{tr}$, $k_{rec}$, and $C_{sc}$, while experimental and calculated values were used for $g_1$, $R$, and $C$. For calculating the Gärtner flux $g_1$, the photon flux has been determined by measuring the light intensity using a UV(A)-meter and subtracting 20% reflection loss.[39] From the resulting value, $g_1$ has been calculated separately for each potential based on the width of the space charge layer and the fraction of photons absorbed within it (see the foregoing section). The $g_1$ values are found to be between $2 \times 10^{-7}$ A and $2.4 \times 10^{-7}$ A $cm^{-2}$ for the (001) face and between $1.1 \times 10^{-7}$ A and $1.3 \times 10^{-7}$ A $cm^{-2}$ for the (100) face at potentials between −0.3 V to 0 V *vs.* Ag/AgCl, respectively. $R$ and $C$ have been extracted from impedance measurements giving $RC$ values between $1 \times 10^{-4}$ and $4 \times 10^{-4}$ $s^{-1}$.

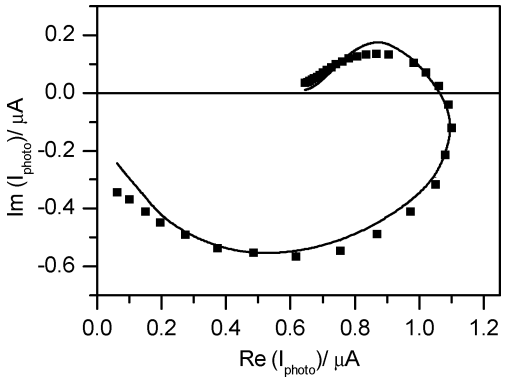


**Fig. 9** Experimental IMPS response measured at the rutile (100) surface (■) in aqueous 0.1 M KCl with a methanol concentration of 1.0% and fitted data (solid line). Applied potential −0.1 V *vs.* AgCl, $g_1 = 10^{-7}$ A cm$^{-2}$, $k_{tr} = 100$ s$^{-1}$, $k_{rec} = 163$ s$^{-1}$, $C_{sc} = 1.2 \times 10^{-6}$ F cm$^{-2}$.

In the following two sections, the $k_{tr}$ and $k_{rec}$ values extracted from the IMPS plots measured at different methanol concentrations and different electrode potentials, respectively, will be discussed.

### Influence of electrode potential

In the simplest case of a one-electron charge transfer process at an ideal surface, the electrode potential is expected to influence the rate of recombination and thereby $k_{rec}$ due to the changing concentration of majority carriers at the electrode surface, but not $k_{tr}$. In the present case, however, changes in the potential clearly lead to changes in both $k_{rec}$ and $k_{tr}$ as seen in Fig. 10 and 11, respectively. This is consistent with the multi-electron charge transfer model presented in the Theory section, since based upon this model $k_{rec}$ and $k_{tr}$ are phenomenological rate parameters, which are both functions of the rate constants associated with the elementary steps of both recombination and charge transfer processes. In the following, the results shown in Fig. 10 and 11 are compared with the potential dependences expected from theory for Case I and Case II.

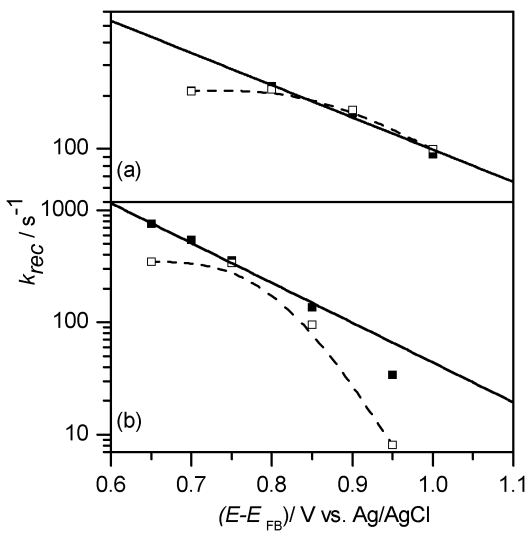


**Fig. 10** Potential dependence of $k_{rec}$ for (a) (001) and (b) (100) surfaces measured with 0 vol% (solid symbols) and 1 vol% (open symbols) methanol in the electrolyte. Solid lines are fits to eqn (7). Dashed lines are for illustration purposes only.

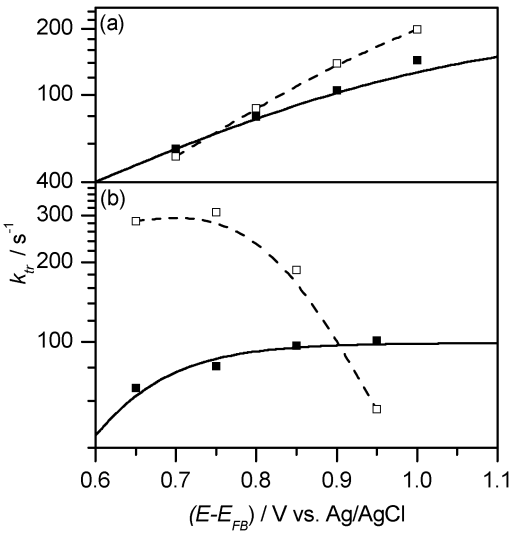


**Fig. 11** Potential dependence of $k_{tr}$ for (a) (001) and (b) (100) surfaces measured at methanol concentrations of 0 vol% (solid symbols) and 1 vol% (open symbols). Solid lines are fits to eqn (6e) with $X_0$ and $k_3$ replaced by eqn (6g) and (7), respectively, and $k_5 = 0$. Dashed lines are for illustration purposes only.

Concerning $k_{rec}$ (Fig. 10), decreasing trends with increasing potential are seen in the case of both (001) and (100) surfaces in the presence as well as in the absence of methanol, which is expected for both Case I and Case II. Based on the approximation that $k_{rec} \approx k_3$ (see Theory) and the fits according to eqn (7) with $E_{FB}$ values taken from the Mott–Schottky plots, the calculations yield $\beta = 0.11 \pm 0.02$ and $k_3^0 = (6.7 \pm 3.1) \times 10^3$ s$^{-1}$ for (001) and $\beta = 0.21 \pm 0.10$ and $k_3^0 = (1.55 \pm 0.6) \times 10^5$ s$^{-1}$ for (100). Note that the fits were made for the $k_{tr}$ values measured in the absence of methanol (solid symbols in Fig. 10), omitting the value measured at −0.3 V *vs.* Ag/AgCl in the case of the (001) surface, since this value clearly deviates from the linear behaviour and is less reliable due to the very small photocurrent at this potential. Both $\beta$ and $k_3^0$ are much lower in the case of the rutile (001) surface, indicating a much higher surface excess charge that can be explained by the population of interband surface states and a much slower recombination rate at this surface.[39]

The $k_{tr}$ values for the (001) face increase towards more positive electrode potentials in the absence of methanol as well as in the presence of 1 vol% methanol (Fig. 11a). This behaviour is typical for Case II, indicating the presence of mobile $OH^{\bullet}_s$ radicals as intermediates in the absence as well as in the presence of methanol. The expected saturation behaviour towards positive potentials is not very distinct under the employed conditions, indicating that the concentration of the $OH^{\bullet}_s$ radicals is not yet saturated at the surface under the employed low light intensity.[37] In the presence of methanol, the $k_{tr}$ values are slightly increased due to $k_5$ becoming $>0$ (eqn (6e)).

For the rutile (100) electrode, the increasing trend of the $k_{tr}$ values towards more positive electrode potentials is only observed in the absence of methanol, this time with a clear saturation behaviour, while a distinct decreasing trend typical for Case I is seen in the presence of 1 vol% methanol (Fig. 11b). This indicates that water oxidation at the (100) face occurs *via*

 

the reaction of two mobile $OH^{\bullet}_s$ radicals, while methanol oxidation mainly involves immobile $OH^{\bullet}_s$ radicals.

While the influence of increasing methanol concentration is analyzed in more detail in the subsequent section, the $k_{tr}$ values measured in the absence of methanol (solid symbols in Fig. 11) have been used to determine $k_4$. For this purpose, these values were fitted to eqn (6e) by replacing $X_0$ by eqn (6g), setting $k_5 = 0$ and considering a potential dependence of $k_3$ according to eqn (7) with $k_3^0$ and $\beta$ fixed to the values determined from Fig. 10. The Gärtner flux $g_1$ was fixed to the range of values calculated from the width of the space charge layer. The resulting $k_4$ values are calculated to be $(4.8 \pm 0.1) \times 10^{-9}$ cm$^2$ s$^{-1}$ and $(9.9 \pm 0.5) \times 10^{-10}$ cm$^2$ s$^{-1}$ for the (001) and the (100) face, respectively.

### Methanol concentration dependence

Fig. 12 shows the methanol concentration dependence of $k_{tr}$ for the two $TiO_2$ surfaces. It is obvious that $k_{tr}$ saturates with increasing methanol concentration at both electrodes. Such a saturation behaviour of $k_{tr}$ is actually expected with increasing $k_5$ (reflecting the increasing methanol concentration) according to eqn (6a) and (e). Therefore, the concentration dependence of $k_{tr}$ has been fitted to eqn (6e) (Case II) in the case of the (001) face and to eqn (6a) (Case I) in the case of the (100) face after replacing $k_5$ by $k_5'$[MeOH] and $X_0$ by eqn (6d) and (g). The $k_5'$ values are $(8.0 \pm 0.6) \times 10^{-9}$ and $(8.0 \pm 0.5) \times 10^{-8}$ cm$^2$ s$^{-1}$ for (001) and (100), respectively. This indicates a clearly faster (by a factor of 10) charge transfer to methanol from immobile $OH^{\bullet}_s$ radicals on the (100) face as compared to the charge transfer from mobile $OH^{\bullet}_s$ radicals on the (001) face.

Similarly, the methanol concentration dependences of $k_{rec}$ have been investigated for the two surfaces, as shown in Fig. 13. Both faces exhibit significantly higher $k_{rec}$ values at small concentrations of methanol, followed by a decrease in $k_{rec}$ with increasing methanol concentration. This decrease with increasing $k_5$ value is expected according to eqn (6b) and (f). Simulation of the results according to eqn (6b) and (f) with the same substitutions for $X_0$ and $k_5$ as mentioned above yielded reasonable fits using the same $k$ values as obtained from the foregoing fits. This can be taken as clear evidence that the chosen model is consistent with the observed concentration dependences of both $k_{tr}$ and $k_{rec}$.

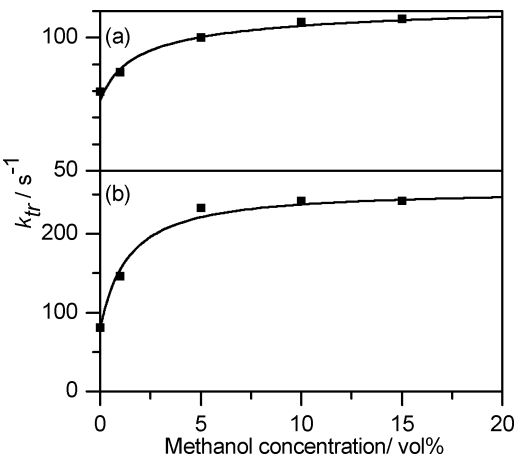


**Fig. 12** Methanol concentration dependence of $k_{tr}$ for rutile (a) (001) and (b) (100) surfaces at −0.2 V *vs.* Ag/AgCl. Lines correspond to fits to eqn (6e) (a) and to eqn (6a) (b), respectively.

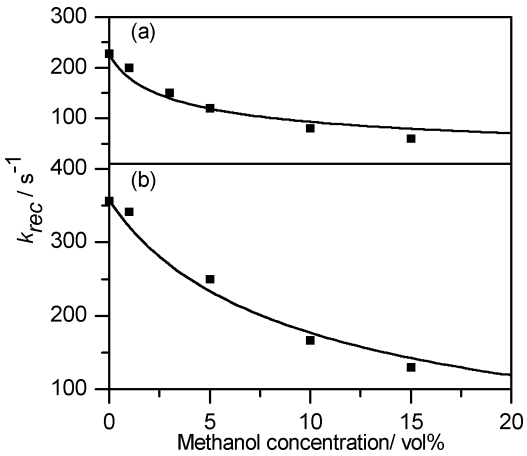


**Fig. 13** Methanol concentration dependence of $k_{rec}$ for rutile (a) (001) and (b) (100) surfaces at −0.2 V *vs.* Ag/AgCl. Lines are simulations corresponding to eqn (6f) (a) and (6b) (b), respectively.

### Correlations between photooxidation mechanisms and surface structures

Like most partially ionic metal oxides, $TiO_2$ exhibits two types of intrinsic ionic surface states associated with unsaturated titanium and oxygen terminal ions, respectively.[41,42] As shown in Fig. 14(a), these surface states are able to electronically interact with electrolyte species, in this case water molecules (hydroxyl ions and protons). The 3d orbitals of 5-fold coordinated terminal titanium cations ($Ti_t$) behave like Lewis acid sites, being able to form strong bonds with the lone electron pairs of hydroxyl ions, while the 2p orbitals of 2-fold coordinated terminal oxygen ions, known as bridging oxygen ($>O^{2-}_{br}$) species, behave like Lewis base sites, being able to share a pair of valence band electrons with the otherwise empty 1s orbitals of $H^+$ cations of the aqueous electrolyte.[43] Assuming dissociative adsorption of water molecules, two types of hydroxyl groups are thus present at the $TiO_2$ surface: adsorbed hydroxyl groups 1-fold coordinated to $Ti_t$ terminal titanium atoms ($OH_t^-$) and bridging hydroxyl ions resulting from the protonation of 2-fold coordinated bridging oxygen ions ($>OH^-_{br}$).[43]

However, there is still a controversy in the literature concerning the nature of the $OH^{\bullet}_s$ radical species initially formed on the $TiO_2$ surface upon illumination. While it is often assumed that the photogenerated free holes in the valence band of $TiO_2$ are trapped by adsorbed $OH_t^-$ ions to produce adsorbed $OH^{\bullet}_t$ radicals, it was recently reported that this process should be kinetically and thermodynamically hindered, because the O 2p energy level of the adsorbed $OH_t^-$ ions is far below the upper valance band edge of $TiO_2$ as confirmed by the analysis of their electronic structure employing metastable impact electron spectroscopy and ultraviolet photoemission spectroscopy.[41,43–46] Therefore, the photogenerated holes should be preferably trapped at bridging 2-fold coordinated terminal oxygen ions ($>OH^-_{br}$), leading to the formation of surface $>OH^{\bullet}_{br}$ radicals as shown in Fig. 14(b).[41,43]

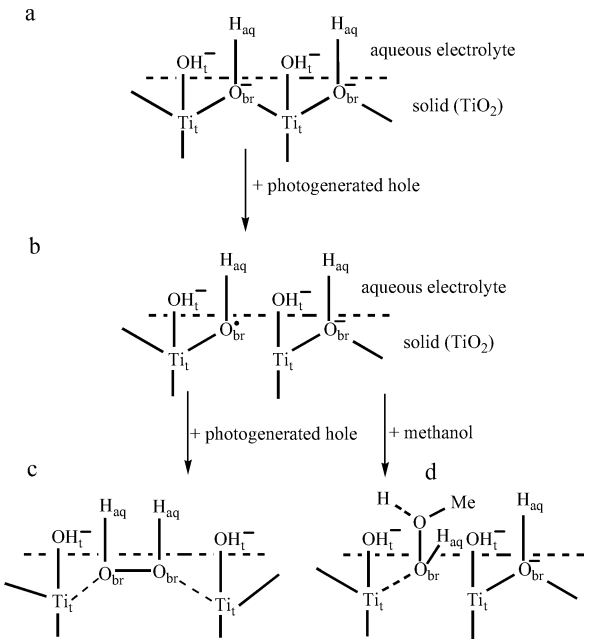


**Fig. 14** Schematic illustration of (a) the two types of surface hydroxyl groups resulting from the dissociative adsorption of water on the $TiO_2$ surface,[43] (b) the preferred trapping position of the photogenerated hole, and (c, d) the different reaction pathways of the photogenerated trapped hole.

In the absence of other oxidizable species such as methanol, two of the photogenerated surface $>OH^{\bullet}_{br}$ radicals react with each other on the (001) surface as well as on the (100) surface as shown in Fig. 14(c). Although bound to specific Ti atoms, these bridging $>OH^{\bullet}_{br}$ radicals therefore behave like mobile $OH^{\bullet}$ radicals under these conditions (Case II in the IMPS model). In the presence of methanol, however, different trends have been observed for the two surfaces. The (001) surface still behaves like in the absence of methanol (Case II), while the same kind of $>OH^{\bullet}_{br}$ radicals behaves like immobile $OH^{\bullet}$ radicals (Case I) on the (100) surface, meaning that the reaction between the two hydroxyl radical intermediates has become negligible. This leads to the conclusion that the photogenerated $>OH^{\bullet}_{br}$ radicals on the (100) surface are more reactive towards methanol oxidation and less reactive towards coupling with another $>OH^{\bullet}_{br}$ radical. This conclusion is in agreement with our finding that the $k_5'$ value, which is representing the charge transfer from the $>OH^{\bullet}_{br}$ radicals to methanol, is 10 times higher on the (100) surface than on the (001) surface, and that the $k_4$ value on the (100) surface is five times smaller than that on the (001) surface. The differences found between the rate constants appear to be reasonable considering the surface structure of both surfaces. (i) The distance between two bridging oxygen anions occupying adjacent positions is 2.54 Å at the (001) face, which is 0.42 Å smaller than the distance of 2.96 Å at the (100) face.[41] Thus, the reaction of two adjacent $>OH^{\bullet}_{br}$ radicals is more likely to occur on the (001) surface than on the (100) surface. (ii) Depending on the atomic alignments on ideal rutile $TiO_2$ (001) and (100) faces, the latter should be considered as a polar surface, whereas the former is nonploar as previously reported.[47,48] Thus, methanol interaction with the (100) surface should be preferred in comparison with that on the (001) surface (Fig. 14d). In fact, it has been reported before that surface trapped holes at 2-fold coordinated $>OH^{\bullet}_{br}$ oxygen ions preferably react with dissolved species that do not interact strongly with the semiconductor surface (*i.e.*, in the absence of specific absorption).[49,50] This is consistent with our observation that the presence of methanol does not lead to a shift in the flatband potential of $TiO_2$, meaning that methanol does not adsorb strongly on the electrode surface. However, the rate of this reaction also seems to depend considerably on the crystallographic orientation of the $TiO_2$ surface, which has not been reported before.

## Conclusions

Intensity modulated photocurrent spectroscopy (IMPS) has been used to investigate the photooxidation of methanol as a model substance for pollutants on rutile $TiO_2$ (001) and (100) surfaces. The values of the phenomenological rate constants $k_{tr}$ and $k_{rec}$ have been determined by a mathematical fit of the experimental IMPS responses using the generalized IMPS equation. The results have been analyzed in view of the influence of the electrode potential, the methanol concentration and the surface structure on the fundamental rate constants of charge transfer and recombination, based on a model that alternatively assumes photooxidation *via* mobile or immobile intermediate radicals. The results indicate that bridging $>OH^{\bullet}_{br}$ radicals, rather than adsorbed $OH^{\bullet}_{t}$ radicals, are involved in water and methanol oxidation on both surfaces. In the absence of methanol, water oxidation proceeds *via* coupling of two bridging $>OH^{\bullet}_{br}$ radicals, making them behave as mobile $OH^{\bullet}$ radicals. In the presence of methanol, water oxidation by coupling of two $>OH^{\bullet}_{br}$ radicals is still the dominating reaction on the (001) surface, while on the (100) surface the trapped holes in the $>OH^{\bullet}_{br}$ radicals are rapidly transferred to methanol, making them appear as immobile $OH^{\bullet}$ radicals. The higher reactivity of the (100) surface towards the photooxidation of methanol and its lower reactivity towards the photooxidation of water are confirmed by corresponding differences in the rate constants and explained by stronger interaction of the polar (100) surface with methanol, as opposed to the non-polar (001) surface, and the larger distance between the $>OH^{\bullet}_{br}$ radicals on the (100) surface, respectively.

## Acknowledgements

A. Y. Ahmed thanks the Egyptian Ministry of Higher Education for providing her a doctoral scholarship (channel system), Sohag University for granting her a leave of absence, as well as Prof. J. Caro at Leibniz Universität Hannover and Prof. F. Raswhan at Sohag University for their support. The authors also thank F. Steinbach, Leibniz Universität Hannover, for the SEM measurements.

## Notes and references

1 M. R. Hoffmann, S. T. Martin, W. Y. Choi and D. W. Bahnemann, *Chem. Rev.*, 1995, **95**, 69–96.
2 I. Bannat, K. Wessels, T. Oekermann, J. Rathousky, D. Bahnemann and M. Wark, *Chem. Mater.*, 2009, **21**, 1645–1653.

 

3 A. A. Ismail, D. W. Bahnemann, I. Bannat and M. Wark, *J. Phys. Chem. C*, 2009, **113**, 7429–7435.
4 A. Bansal and N. S. Lewis, *J. Phys. Chem. B*, 1998, **102**, 1067–1070.
5 S. Somasundaram, C. R. N. Chenthamarakshan, N. R. de Tacconi and K. Rajeshwar, *Int. J. Hydrogen Energy*, 2007, **32**, 4661–4669.
6 J. N. Nian, C. C. Hu and H. Teng, *Int. J. Hydrogen Energy*, 2008, **33**, 2897–2903.
7 M. Kitano, K. Tsujimaru and M. Anpo, *Top. Catal.*, 2008, **49**, 4–17.
8 L. M. Peter and D. Vanmaekelbergh, *Advances in Electrochemical Science and Engineering*, Wiley-VCH, Weinheim, 1999.
9 W. J. Albery, N. L. Dias and C. P. Wilde, *J. Electrochem. Soc.*, 1987, **134**, 601–609.
10 L. M. Peter, *Chem. Rev.*, 1990, **90**, 753–769.
11 K. Rajeshwar, *J. Electrochem. Soc.*, 1982, **129**, 1003–1008.
12 J. J. Kelly and R. Memming, *J. Electrochem. Soc.*, 1982, **129**, 730–738.
13 K. Schwarzburg and F. Willig, *J. Phys. Chem. B*, 1997, **101**, 2451–2458.
14 B. B. Smith and A. J. Nozik, *J. Phys. Chem. B*, 1997, **101**, 2459–2475.
15 T. Oekermann, D. Schlettwein and N. I. Jaeger, *J. Electroanal. Chem.*, 1999, **462**, 222–234.
16 J. N. Chazalviel, *J. Electrochem. Soc.*, 1982, **129**, 963–969.
17 W. J. Albery, P. N. Bartlett and C. P. Wilde, *J. Electrochem. Soc.*, 1987, **134**, 2486–2491.
18 J. Schefold, *J. Electroanal. Chem.*, 1992, **341**, 111–136.
19 A. D. Modestov, G. D. Zhou, H. H. Ge and B. H. Loo, *J. Electroanal. Chem.*, 1994, **375**, 293–299.
20 A. Goossens, *Surf. Sci.*, 1996, **365**, 662–671.
21 G. Oskam, J. C. Schmidt and P. C. Searson, *J. Electrochem. Soc.*, 1996, **143**, 2538–2543.
22 G. Schlichthörl, N. G. Park and A. J. Frank, *Z. Phys. Chem.*, 1999, **212**, 45–50.
23 P. E. de Jongh and D. Vanmaekelbergh, *J. Phys. Chem. B*, 1997, **101**, 2716–2722.
24 O. A. Semenikhin, V. E. Kazarinov, L. Jiang, K. Hashimoto and A. Fujishima, *Langmuir*, 1999, **15**, 3731–3737.
25 T. Oekermann, D. Schlettwein and N. I. Jaeger, *J. Phys. Chem. B*, 2001, **105**, 9524–9532.
26 R. Peat and L. M. Peter, *J. Electroanal. Chem.*, 1987, **228**, 351–364.
27 J. Taranto, D. Frochot and P. Pichat, *Ind. Eng. Chem. Res.*, 2009, **48**, 6229–6236.
28 J. Taranto, D. Frochot and P. Pichat, *Sep. Purif. Technol.*, 2009, **67**, 187–193.
29 L. Liu, A. Chakma, X. S. Feng and D. Lawless, *Can. J. Chem. Eng.*, 2009, **87**, 456–465.
30 A. Imanishi, H. Suzuki, K. Murakoshi and Y. Nakato, *J. Phys. Chem. B*, 2006, **110**, 21050–21054.
31 A. Imanishi, H. Suzuki, N. Ohashi, H. Kondoh, T. Ohta and Y. Nakato, *J. Phys. Chem. C*, 2009, **113**, 17254–17261.
32 W. W. Gartner, *Phys. Rev.*, 1959, **116**, 84–87.
33 E. A. Ponomarev and L. M. Peter, *J. Electroanal. Chem.*, 1995, **396**, 219–226.
34 L. Z. Sun and J. R. Bolton, *J. Phys. Chem.*, 1996, **100**, 4127–4134.
35 C. Y. Wang, J. Rabani, D. W. Bahnemann and J. K. Dohrmann, *J. Photochem. Photobiol., A*, 2002, **148**, 169–176.
36 J. Marugan, D. Hufschmidt, M. J. Lopez-Munoz, V. Selzer and D. Bahnemann, *Appl. Catal., B*, 2006, **62**, 201–207.
37 L. M. Peter, E. A. Ponomarev and D. J. Fermin, *J. Electroanal. Chem.*, 1997, **427**, 79–96.
38 D. J. Fermin, E. A. Ponomarev and L. M. Peter, in *Proceedings of the Symposium on Photoelectrochemistry*, Electrochemical Society Inc, Pennington, 1997, vol. 97, pp. 62–71.
39 L. Kavan, M. Gratzel, S. E. Gilbert, C. Klemenz and H. J. Scheel, *J. Am. Chem. Soc.*, 1996, **118**, 6716–6723.
40 P. Salvador, *J. Appl. Phys.*, 1984, **55**, 2977–2985.
41 P. Salvador, *Prog. Surf. Sci.*, 2011, **86**, 41–58.
42 S. R. Morrison, *Electrochemistry at Semiconductor Electrodes and Oxide Metal Electrodes*, Plenum Press, New York, 1981.
43 P. Salvador, *J. Phys. Chem. C*, 2007, **111**, 17038–17043.
44 R. L. Kurtz, R. Stockbauer, T. E. Madey, E. Roman and J. L. Desegovia, *Surf. Sci.*, 1989, **218**, 178–200.
45 S. Krischok, O. Hofft, J. Gunster, J. Stultz, D. W. Goodman and V. Kempter, *Surf. Sci.*, 2001, **495**, 8–18.
46 J. Felipe Montoya, J. Peral and P. Salvador, *ChemPhysChem*, 2011, **12**, 901–907.
47 R. Wang, N. Sakai, A. Fujishima, T. Watanabe and K. Hashimoto, *J. Phys. Chem. B*, 1999, **103**, 2188–2194.
48 V. E. Henrich and R. L. Kurtz, *Phys. Rev. B: Condens. Matter Mater. Phys.*, 1981, **23**, 6280–6287.
49 T. L. Villarreal, R. Gomez, M. Gonzalez and P. Salvador, *J. Phys. Chem. B*, 2004, **108**, 20278–20290.
50 D. Monllor-Satoca, R. Gomez, M. Gonzalez-Hidalgo and P. Salvador, *Catal. Today*, 2007, **129**, 247–255.